2022 Asia Communications and Photonics Conference (ACP) and International Conference on Information Photonics and Optical Communications (IPOC)

Photonics-aided Multi-subcarrier Phase-insensitive/Sensitive PAM-4 Multiplexing Wireless Transmission System at 100 GHz

Weidong Tong, Jiao Zhang*, Min Zhu*, Weiliang Xu, Yingxin Wei, Shuang Gao, Qinru Li, Xiang Liu,
National Mobile Communications Research Laboratory
Southeast University
Nanjing 210096, China
e-mail: jiaozhang@seu.edu.cn; minzhu@seu.edu.cn

Bingchang Hua, Mingzheng Lei, Yuancheng Cai, Liang Tian, Yucong Zou
Center for Pervasive Communications
Purple Mountain Laboratories
Nanjing, 211111, China

2022 Asia Communications and Photonics Conference (ACP) | 978-1-6654-8155-7/22/$31.00 ©2022 IEEE | DOI: 10.1109/ACP55869.2022.10089068

***Abstract*—We demonstrate 46 Gb/s 4-subcarrier PAM-4 signals generation and THz wave wireless transmission at 100-GHz, enabled by intensity modulation and heterodyne coherent detection. A comprehensive comparison of phase-insensitive scheme and phase-sensitive scheme is investigated. The simulation results show that the phase-sensitive scheme has a 5.5 dB received optical power sensitivity improvement and 1.8 dB input optical power into photodiode (PD) sensitivity improvement compared with phase-insensitive scheme.**

Keywords—THz, subcarrier multiplexing, PAM-4, phase insensitive, phase sensitive

I. Introduction

The advantages of the enormous amount of available spectrum and the good directionality of THz-wave will make high-speed terahertz-wave (THz-wave, 0.1–10 THz) wireless transmission an unavoidable trend in the upcoming 6G [1-4]. The bandwidth constraint of all-electrical methods is a problem that photonics-assisted THz-wave generation technology successfully addresses [5] when considering the bottleneck in electrical devices. There are several typical techniques which can be used to realize large-capacity fiber-optic transmission, including optical polarization multiplexing, high-level modulation format, multi-carrier modulation, as well as advanced transmitter-end and receiver-end DSP algorithms [6].

In 2020, Karlsruhe Institute of Technology (KIT) demonstrated a net data rate of 115 Gbit/s wireless transmission at a carrier frequency of 0.3 THz over a distance of 110 m with a Schottky-barrier diode and Kramers-Kronig scheme [7]. In 2021, Japan scientists successfully transmitted 32-/64-QAM OFDM and single-carrier signal with a record line rate of 71.4 Gb/s and net data rate of 53.7 Gb/s using low loss optical modulator and direct photonic down-conversion [8]. In 2022, Technical University of Denmark conducted an experimental demonstration of a single channel, 10.7 m-long, 131.21 Gbit/s net rate THz-band wireless transmission using 16-QAM-OFDM modulation, nonlinear DSP flow, and an injection-locked heterodyne THz generator based on photonic integrated circuits (PIC) made by a generic foundry [9]. These studies, however, primarily rely on heterodyne coherent detection and vector modulation, which need pricey I/Q modulation, raising system costs and DSP complexity. At present, researches based on intensity modulation and heterodyne coherent detection mainly focus on the field of coherent passive optical network (PON) [10] and photonics-aided mm-wave transmission [11]. But the the viability of heterodyne detection and intensity modulation in THz-wave communication with photonic-aided has not been thoroughly investigated. Furthermore, the above studies mainly use single-carrier (SC) modulation, which are largely affected by chromatic dispersion (CD) and nonlinear effect of fiber and has limited rate. Subcarrier multiplexing (SCM) technique is a popular approach to provide multi-gigabit mobile data transmission for photonics-aided THz-wave signal delivery. Adopting SCM technique can reduce the signal baud rate and bandwidth requirement for devices. Moreover, SCM technique has a better tolerance to the spectrum fading effect, hence its introduction into the THz-wave signal delivery can further improve the performance. In this paper, we simulate a 46 Gbit/s PAM-4 signal wireless transmission system at 100 GHz based on 4-subcarrier multiplexing (SCM-4), and two schemes by phase-insensitive/sensitive PAM-4 are discussed.

II. Principle

A. Subcarrier Multiplexing and De-multiplexing

According to related studies, coherent optical (CO) transmission systems' nonlinear performance is significantly influenced by the subcarrier granularity [11–14]. Even though SCM signals typically have a higher peak-to-average power ratio (PAPR), the nonlinearity and CD tolerance of the system can be improved by multiplexing the high-baud-rate SC signal into numerous low-baud-rate subcarriers and optimizing the number of subcarriers [13]. This increased tolerance can be explained by the four wave mixing efficiency theory or the walk-off between subcarriers due to CD [14]. On the other hand, SCM signals may now be easily obtained thanks to the fast development of high-speed digital-to-analog converters (DAC) by creating the necessary signals digitally in the transmitter DSP and loading the samples to DACs for digital-to-analog conversion. In addition, it is worth noting that the implementation penalty is anticipated to be lower compared to the analog approaches since the multiplexing of subcarriers is accomplished in the digital domain [15]. Besides, SCM can fully utilize the bandwidth of the electrical channel to maximize the system capacity. The schematic diagram of SCM is shown in Fig. 1. Baseband signals are modulated on microwaves with different frequencies and then multiplexed. The multiplexed signals are modulated on an optical carrier, and injected into fiber. At the receiver side, photoelectric conversion is operated by a photoelectric detector (PD).

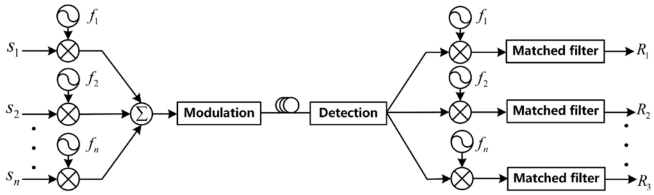

Figure 1. The schematic diagram of SCM.

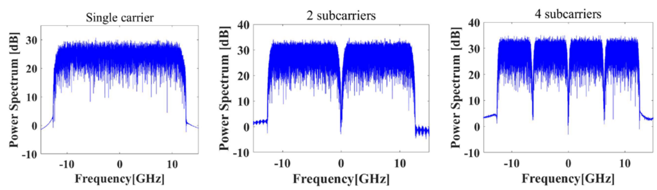

Figure 2. Power spectrum of the SC signal and SCM signals.

Matched filters are used for de-multiplexing, and then each signal is processed independently for recovery. The transmitter-side spectrum of the SC signal and the SCM transmissions with 2 and 4 subcarriers are shown in Fig. 2. The two SCM signals' respective subcarrier baud rates are 11.5 GBaud and 5.75 GBaud based on the 23 GBaud total baud rate. Each subcarrier uses the PAM-4 modulation scheme. The pulse shaping method is root raised cosine (RRC) with a roll-off factor of 0.1. The optical bandwidth and spectral efficiency are the same for all signals in the SCM signal spectrum because there is no guard band remaining between subcarriers.

B. Phase-insensitive/Sensitive PAM-4 Signal

Figure 3 shows the electrical field and power transfer function curves in which two operating points along the power transfer curve that are worth mentioning. The input voltage swing is V_π and the output power is half of the maximum power (normalized power) which corresponding to the quadrature points (V_{bias}=$-V_\pi/2$ or $V_\pi/2$). Another one is the null point (V_{bias}= $-V_\pi$ or V_π), which has an output power of zero and an input voltage swing of $2V_\pi$. When the input voltage reaches the null point of the MZM, there may be not only amplitude modulation but also a phase skip of if the MZM is biased at the null point. Therefore, phase recovery is required in the DSP at the receiver side. The field and power transfer functions are nonlinear. Distortion can be avoided when the input voltage fluctuation at the null point is less than 2V_π, although this leads to large optical losses. If the MZM is biased at the quadrature point, pure amplitude modulation exists to avoid phase recovery, but the linear region is relatively small and the optical signal-to-noise ratio (OSNR) sensitivity is relatively lower than for null point. In this work, we set the MZM bias to null point considering with the OSNR performance and DSP complexity.

At the transmitter, PAM-4 signal can be classified into phase-insensitive and phase-sensitive cases based on different mapping relations. For the former, the PAM-4 signal level is located at {0, 1, 2, 3}, and the constellation will convergence into four rings which is shown in Fig. 4 (a) due to laser phase noise. This scheme does not need phase recovery because each ring represents one symbol. As shown in Fig. 4(b), for the latter, the constellation will converge into two rings with the PAM-4 signal level at {-3, -1, 1, 3} where {-3, 3} and {-1, 1} have the same modulus. Thus, phase recovery is required before a decision is made on the phase-sensitive scheme, which is similar to a standard IQ modulated coherent detection system, except that no orthogonal dimensions are used to encode the information.

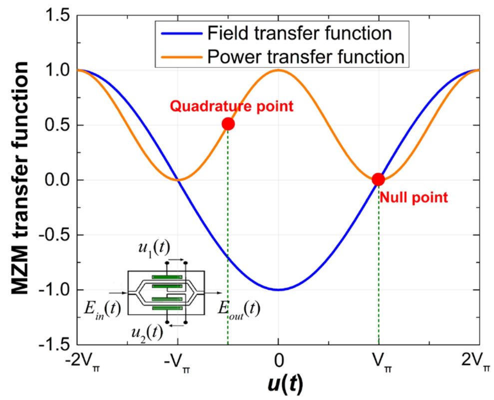

Figure 3. Field and power transfer functions of the MZM modulator

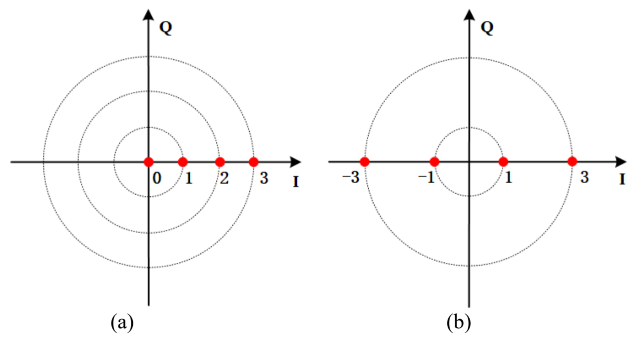

Figure 4. (a) Constellation of phase-insensitive PAM-4; (b) Constellation of phase-sensitive PAM-4

C. Digital Signal Processing

The transmitter side DSP flow is shown in Fig.5(a). The bit sequence is first mapped into PAM-4 symbols, while {0, 1, 2, 3} is used for phase-insensitive case and {-3, -1, 1, 3} is used for phase-sensitive case. Then, serial-to-parallel conversion is applied to generate n signals. Each signal is filtered by a root raised cosine (RRC) filter to realize nyquist pulse shaping. Finally, each output is multiplexed after being shifted to distinct frequencies in the spectrum.

The off-line DSP flow for PAM-4 symbol recovery at the receiver side is shown in Fig. 5(b). Optical transmission impairments can be compensated by using DSP in the electrical domain. The received SCM signals are first down-converted to baseband by frequency shifting with low-pass filtering to eliminate the out-of-band amplified spontaneous emission (ASE) noise, and then resampled to twice the total baud rate. A single detection simultaneously captures every subcarrier. Each subcarrier is sequentially shifted to baseband after the frequency domain transform and filtered out with an RRC matching filter. The low-baud-rate signal in each subcarrier is then translated to time domain and put through parallel processing, including squaring timing recovery to compensate for the difference between the symbol clock and the ADC sample clock, channel equalization to mitigate inter-symbol interference (ISI), and carrier recovery to recover the phase which is needed for the phase-sensitive scheme. Finally, PAM-4 symbol de-mapping and BER calculation are operated.

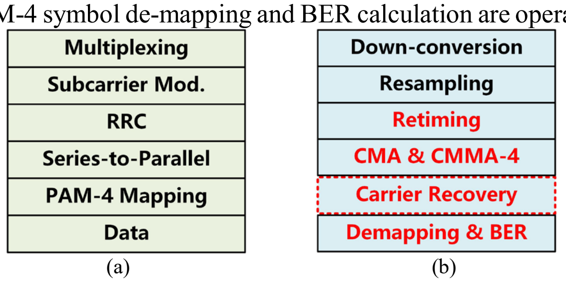

Figure 5. (a) Transmitter DSP; (b) Receiver DSP.

III. Simulation Setup

The simulation setup for our demonstrated 46 Gb/s multi-subcarrier PAM-4 wireless transmission using intensity modulation and heterodyne coherent detection is shown in Fig. 6. First, the central office generates SCM-4 signals offline at a total baud rate of 23 GBaud. For each subcarrier, the roll-off factor of the RRC pulse shaping filter is set to 0.4, and there is no guard band. The SCM-4 signal is used to drive the MZM after a 92 GSa/s DAC conversion and enhancement of an electronic amplifier (EA). A half-wave voltage of 4V is used to bias MZM at the null point. Continuous wave (CW) from an external cavity laser (ECL-1) is used to carry the SCM-4 signal with a wavelength of 1553.6 nm. Meanwhile, the ECL-2 at base station operates as a local oscillator (LO) with an output wavelength of 1552.8 nm.

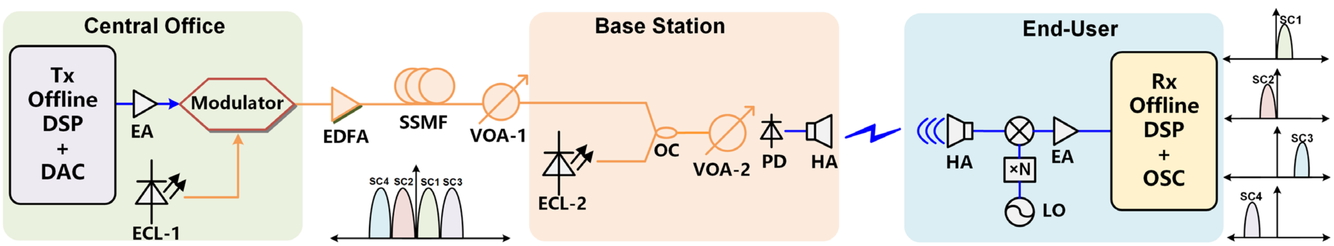

Figure 6. Simulation setup for a 46 Gb/s multi-subcarrier PAM-4 wireless transmission simulation using intensity modulation and heterodyne detection.

ECL-1 and ECL-2 have a frequency separation of 100 GHz, and their linewidths are both 5 MHz. Prior to entering the fiber, an optical signal is amplified by one erbium doped fiber amplifier (EDFA). A variable optical attenuator (VOA-1) is used to control the received optical power for sensitivity evaluation after a 25 km standard single-mode fiber (SSMF) transmission. VOA-2 is used to adjust the input optical power into PD after combining with LO via an optical coupler (OC). By using heterodyne beating, the PD is utilized for the generation of 0.1-THz wireless signals. The signal is wirelessly transmitted via a pair of horn antennas (HAs). It should be noted that we only evaluate back-to-back wireless transmission. An 80-GHz sinusoidal RF source, a mixer, and analog down-conversion are used at the end user's side. Following that, the down-converted intermediate-frequency (IF) signal is then enhanced by another EA and collected by an 80 GSa/s oscilloscope for offline processing, which is illustrated in Fig. 5. (b).

IV. Results and Discussion

We simulated 23-GBaud SCM-4 wireless transmission with phase insensitive and phase sensitive PAM-4 signals. In the SCM signal spectra, no guard band is left between subcarriers, and the bandwidth is 32.2 GHz when the nyquist pulse shaping roll-off factor is about 0.4. Fig. 7 depicts the power spectrum of transmitted SCM-4 signals for phase-insensitive scheme. It can be observed that every subcarrier is added with a DC component due to asymmetrical PAM-4 mapping. Resampling and retiming are used at the receiver, and the related constellation diagrams for both the real and image parts are shown in Fig. 8(a) and (b). It can be seen that four concentric rings constellation is obtained in Fig. 8(c), which corresponds to the case where the CMMA equalizer is employed. Symbol decision can be made directly because there is no information conveyed on the phase.

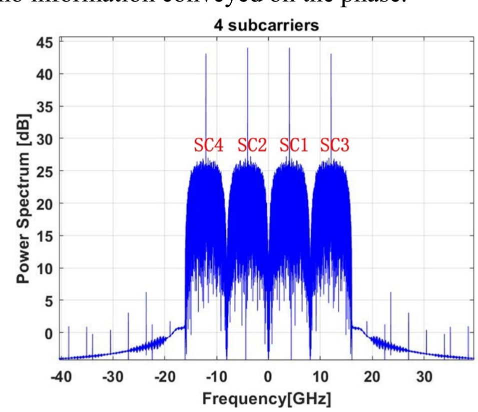

Figure 7. The power spectrum of transmitted SCM-4 signals with phase-insensitive PAM-4

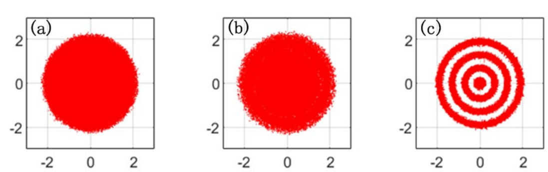

Figure 8. Constellations after (a) resampling; (b) retiming; (c) channel equalization

For phase-sensitive PAM-4 scheme, the power spectrum of transmitted SCM-4 signals is shown in Fig. 9. It can be observed that every subcarrier has no DC component due to symmetrical PAM-4 mapping. At the received side, after down-conversion, resampling and retiming, we use the CMMA equalization with two reference circles and two concentric rings constellation as shown in Fig. 10, (c). After coherent detection, phase noise induced by two laser linewidths and frequency offset is introduced into the received signals. The VVPE algorithm removes phase rotation caused by laser frequency offset and phase noise. Figures 10(d) and 10(e) depict the symbol pattern following FOE and CPE, respectively. Finally, the symbol decision and BER calculation are performed.

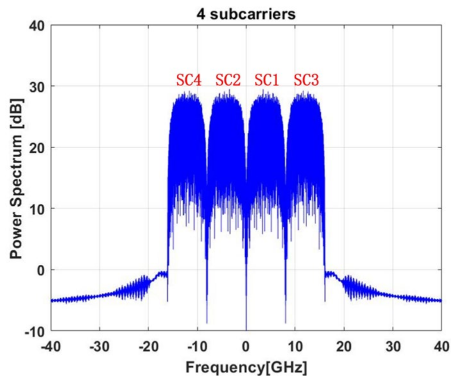

Figure 9. The power spectrum of transmitted SCM-4 signals by phase-sensitive PAM-4

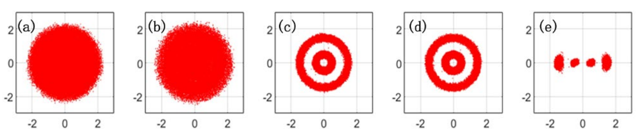

Figure 10. Constellations after (a) resampling; (b) retiming; (c) channel equalization; (d) FOE; (e) CPE.

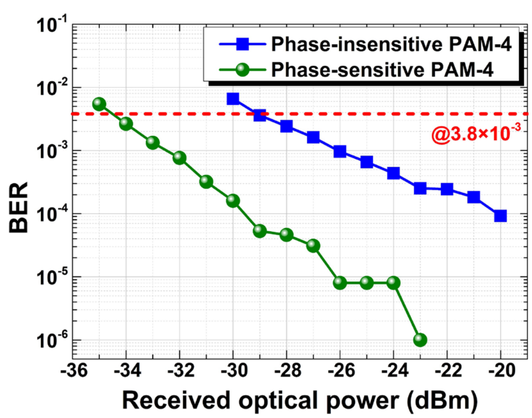

Figure 11. BER versus received optical power under different mapping schemes

Fig. 11 gives the measured BER performances versus received optical power under two mapping schemes including phase-insensitive PAM-4 and phase-sensitive PAM-4. In both phase-insensitive and phase-sensitive schemes, it is obvious that BER performances improve as received optical power increases. The phase-sensitive scheme outperforms the phase-insensitive scheme which is due to two factors. Firstly, phase-sensitive PAM-4 signal has no DC component interference. Secondly, the Euclidean distance of phase-insensitive PAM-4 constellation is larger. The received optical power for phase-insensitive and phase-sensitive scheme is about -29 dBm and -34.5 dBm at 3.8×10^{-3}. Compared with phase-insensitive scheme, the phase-sensitive scheme can obtain about 5.5 dB received optical power sensitivity gain.

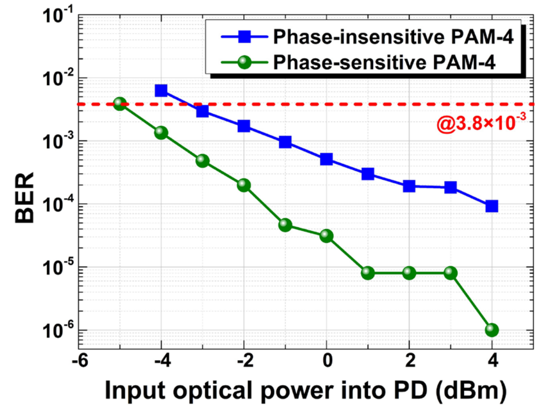

Figure 12. BER versus input optical power into PD under different mapping schemes

Fig. 12 shows that the input optical power into PD for phase-insensitive and phase-sensitive scheme is about -3.2 dBm and -5 dBm at 3.8×10^{-3}. The phase-sensitive scheme obtains about 1.8 dB input optical power into PD sensitivity gain compared with phase-insensitive scheme. However, the receiver sensitivity gain is improved at the expense of DSP complexity, which adds the carrier recovery module.

V. Conclusion

In this paper, a 46 Gbit/s PAM-4 signal wireless transmission system at 100 GHz based on SCM-4 is proposed and simulated. We evaluated the BER for both phase-insensitive scheme and phase-sensitive schemes, respectively. The simulation results show that the phase-sensitive scheme can provide better performance because it has no DC component interference and its Euclidean distance is larger compared with phase-insensitive scheme. The phase-sensitive scheme has a 5.5 dB received optical power sensitivity improvement and 1.8 dB input optical power into PD sensitivity improvement compared with phase-insensitive scheme. However, the improved performance comes at the expense of DSP complexity that the carrier recovery module is added for phase-sensitive scheme. Compared with vector modulation, these two schemes both decrease DSP complexity and improve the tolerance to CD and nonlinear effect of fiber.

Acknowledgment

This research was supported in part by the National Natural Science Foundation of China (Grant Nos. 62101121 and 62101126), the Open Fund of IPOC (BUPT, IPOC2021A01), the project (2021M702501,2022T150486) funded by China Postdoctoral Science Foundation, Key Research and Development Program of Jiangsu Province (BE2020012), and the open project (2022GZKF003) of the State Key Laboratory of Advanced Optical Communication Systems and Networks, Shanghai Jiao Tong University.

REFERENCES

[1] Nagatsuma T. THz communication systems[C]//Optical Fiber Communication Conference. Optica Publishing Group, 2017: Tu3B. 1.

[2] Li X, Yu J, Wang K, et al. Photonics-aided 2× 2 MIMO wireless terahertz-wave signal transmission system with optical polarization multiplexing[J]. Optics Express, 2017, 25(26): 33236-33242.

[3] Zhou W, Zhao L, Chen Y W, et al. W-band PAM-4 wireless delivery employing intensity modulation and coherent detection based on CMMA equalization[C]//2019 IEEE MTT-S International Microwave Conference on Hardware and Systems for 5G and Beyond (IMC-5G). IEEE, 2019: 1-3.

[4] Zhou W, Zhao L, Zhang J, et al. 135-GHz D-band 60-Gbps PAM-8 wireless transmission employing a joint DNN equalizer with BP and CMMA[J]. Journal of Lightwave Technology, 2020, 38(14): 3592-3601.

[5] Yu J. Photonics-assisted millimeter-wave wireless communication[J]. IEEE Journal of Quantum Electronics, 2017, 53(6): 1-17.

[6] Li X, Yu J, Chang G K. Photonics-assisted technologies for extreme broadband 5G wireless communications[J]. Journal of Lightwave Technology, 2019, 37(12): 2851-2865.

[7] Harter T, Füllner C, Kemal J N, et al. Generalized Kramers–Kronig receiver for coherent terahertz communications[J]. Nature Photonics, 2020, 14(10): 601-606.

[8] Dat P T, Yamaguchi Y, Inagaki K, et al. Transparent fiber–radio–fiber bridge at 101 GHz using optical modulator and direct photonic down-conversion[C]//2021 Optical Fiber Communications Conference and Exhibition (OFC). IEEE, 2021: 1-3.

[9] Jia S, Lo M C, Zhang L, et al. Integrated dual-laser photonic chip for high-purity carrier generation enabling ultrafast terahertz wireless communications[J]. Nature communications, 2022, 13(1): 1-8.

[10] Zhang J, Yu J, Li X, et al. 200 Gbit/s/λ PDM-PAM-4 PON system based on intensity modulation and coherent detection[J]. Journal of Optical Communications and Networking, 2020, 12(1): A1-A8.

[11] Du L B, Lowery A J. Optimizing the subcarrier granularity of coherent optical communications systems[J]. Optics express, 2011, 19(9): 8079-8084.

[12] Bononi A, Rossi N, Serena P. Performance dependence on channel baud-rate of coherent single-carrier WDM systems[C]//39th European Conference and Exhibition on Optical Communication (ECOC 2013). IET, 2013: 1-3.

[13] Shieh W, Tang Y. Ultrahigh-speed signal transmission over nonlinear and dispersive fiber optic channel: the multicarrier advantage[J]. IEEE Photonics Journal, 2010, 2(3): 276-283.

[14] Tang Y, Shieh W, Krongold B S. DFT-spread OFDM for fiber nonlinearity mitigation[J]. IEEE Photonics Technology Letters, 2010, 22(16): 1250-1252.

[15] Zhu Y, Wang J, Guo Q, et al. Experimental comparison of Terabit Nyquist superchannel transmissions based on high and low baud rates[C]//2013 Optical Fiber Communication Conference and Exposition and the National Fiber Optic Engineers Conference (OFC/NFOEC). IEEE, 2013: 1-3.